

Landslides (2019) 16:1327–1340
 DOI 10.1007/s10346-019-01164-0
 Received: 6 September 2018
 Accepted: 1 March 2019
 Published online: 9 April 2019
 © Springer-Verlag GmbH Germany
 part of Springer Nature 2019

H. Y. Luo · L. L. Zhang · L. M. Zhang

Progressive failure of buildings under landslide impact

Abstract Buildings are the most concerned element in landslide risk assessment. A weak link in landslide risk analysis is the evaluation of building response and vulnerability when impacted by a landslide. In this paper, failure mechanisms and processes of typical reinforced concrete buildings upon landslide impacts are discovered through an explicit time integration analysis in LS-DYNA. The Arbitrary Lagrangian–Eulerian formulation, which allows automatic rezoning, is applied to simulate the landslide flow dynamics and the impact into the building. Three landslide intensity levels are considered. Progressive collapse of the building is observed in the high-impact intensity case. The frontal walls are firstly destroyed due to its low out-of-plane flexural capacity, followed by the progressive failure of columns at the ground floor. The collapse of building occurs when the remaining load-bearing components cannot resist the superstructure loadings. Two plastic hinge failure mechanisms are observed on the damaged columns when the ultimate bending moments of the columns are exceeded at both ends. Finally, a five-class classification system is proposed to evaluate building damage states based on field observations and the numerical simulation results. The analysis helps robust building design and assessment of building vulnerability to landslides.

Keywords Landslides · Debris flow · Buildings · Vulnerability · Impact analysis · Progressive failure · LS-DYNA

Introduction

Rainfall- or earthquake-induced landslides can be destructive events when they mobilize large volumes of soil and/or rock and undergo large distances. It is impossible to stop such disastrous events of the nature; the only way is to reduce or avoid the risk (Tiwari and Marui 1999). In such a case, risk mitigation measures must necessarily focus on the vulnerability of the exposed elements and, in particular, of the buildings potentially impacted by landslides, as the destruction of buildings can not only cause enormous economic losses but also endanger the people inside the buildings. Corominas et al. (2014) performed comprehensive quantitative landslide risk assessment and noted that the vulnerability assessment, which is a key component of landslide risk assessment, has been limited. A significant research gap exists in assessing the vulnerability of buildings exposed to landslides (Mavrouli et al. 2014).

Existing methods to assess the damage of building structures can be divided into the following three categories: expert judgment or factor-related method (Leone et al. 1996; Uzielli et al. 2008; Li et al. 2010; Uzielli et al. 2015), statistical methods based on past failure data (Fuchs et al. 2007; Akbas et al. 2009; Totschnig and Fuchs 2013; Quan Luna et al. 2011; Lo et al. 2012; Jakob et al. 2012; Eidsvig et al. 2014; Kang and Kim 2016; Peduto et al. 2017; Zhang et al. 2018), and physically based numerical simulations (Mavrouli and Corominas 2010a, 2010b; Negulescu and Foerster 2010; Fotopoulou and Pitilakis 2013; Parisi and Sabella 2017). Among these methods, statistical methods are the most frequently used in

the literature. Despite the progress in the assessment of building vulnerability to landslides, some important aspects are still missing in the statistical methods. First, the accuracy of the statistical methods is highly data-dependent and some important data about landslide intensity and structure damage state are very hard to retrieve from past failure events. Second, the explicit interaction process between landslide intensity and building damage is not considered. Many uncertainties are involved in the interaction process. Particular characteristics of buildings, such as the structure type, material property, geometry, and position, are not considered, so that the building damage is often expressed as monetary loss. Few are expressed as physical damage. If any, the damage states of building are classified in a qualitative way (e.g., Jakob et al. 2012; Kang and Kim 2016). Third, the landslide intensity is often expressed as the debris depth as it can be obtained easily from field surveys. Other intensity measures, such as velocity or pressure, are rarely available in the literature.

A prerequisite for the establishment of a physical vulnerability model is to understand the interaction process and failure mechanisms of building structures. An explicit physical meaning can, then, be provided to enhance the structural design and reduce the vulnerability of building structures. Mavrouli and Corominas (2010a, 2010b) have utilized a finite element model to analyze the dynamic response of buildings subjected to rockfall. Buildings exposed to slow-moving landslides have been studied in a numerical method by Fotopoulou and Pitilakis (2013). As for the rapid flow-like landslide, Faella and Nigro (2003a, 2003b) performed pioneering work on the failure mechanisms of buildings based on field studies. Federico and Amoroso (2008) applied a uniform hydrodynamic pressure on the whole height of an RC pillar to back analyze the column failure mechanism proposed by Faella and Nigro (2003a). Mavrouli et al. (2014) presented a method to assess the vulnerability of simple reinforced concrete buildings based on limit state theory. More recently, Parisi and Sabella (2017) carried out fragility analysis for RC-framed buildings and masonry infill walls using pushover analysis. A distributed landslide impact pressure was applied to the structure directly, which was assumed to consist of a hydrostatic pressure and a dynamic overpressure. Yet, the impact process between the landslide and the building is not considered. It is still a challenge to predict the progressive collapse process of buildings impacted by landslides or debris as a complex dynamic interaction process (Zeng et al. 2015). The progressive failure mechanisms of the building structure must be explored further and verified with field evidence.

In this paper, a numerical method is applied to investigate the landslide–building interaction and building failure process. The structural responses and progressive collapse mechanisms of typical RC-framed buildings are analyzed. In the following, the numerical models are described in the “Analysis methodology” section. Then, the progressive collapse processes and failure mechanisms are analyzed in the “Progressive building collapse processes” and “Failure mechanisms of

building components” sections. Finally, a five-class classification system is proposed to assess the building damage state.

Analysis methodology

Numerical model

Numerical simulation of the complex interaction between a landslide and a building is still a challenging task, especially when large deformations are involved. LS-DYNA is a multi-purpose finite element platform; its contact algorithms and fluid–structure interaction module are suitable for dealing with the complex interaction problems. Kwan et al. (2015) and Koo et al. (2017) have utilized this package to analyze landslide flow and landslide–barrier interaction problems. It has been shown to provide good predictions of landslide mobility and landslide–structure interactions. More importantly, it provides an algorithm to simulate the complicated behavior of reinforced concrete components. Therefore, an explicit dynamic analysis of progressive collapse of a three-dimensional reinforced concrete (RC)-framed building structure due to landslide impact is carried out.

In this impact simulation, three parts need to be modeled—landslide, RC-framed building structure, and terrain, which are shown in Fig. 1. The landslide is modeled using 8-node solid elements with one integration point. The Arbitrary Lagrangian–Eulerian (ALE) formulation, which can perform automatic rezoning and handle scalar advection in an Eulerian grid, is applied to the solid elements of landslide (Hallquist 2006). The terrain is modeled using rigid solid elements. The RC-framed building structure can be simulated by both implicit and explicit models. In an implicit model, the reinforced concrete is regarded as a homogenous material in which the concrete and rebar are treated as a whole. Generally, an implicit

method, using beam and shell elements, is more efficient and most commonly used to analyze the global structure response in the literature, for example, under seismic loading (Lin et al. 2014) or blast loading (Almusallam et al. 2010). However, as Elsanadedy et al. (2014) mentioned, the employment of beam elements for columns and beams may create problems in the application of blast pressure, which means the two-node beam elements cannot be well coupled with ALE elements and the loads on columns are only transmitted through the façade elements. In this way, the column and beam failure, which is a critical failure phenomenon in the building damage evaluation, cannot be well captured. Therefore, in this paper, the explicit model is applied considering its accuracy.

In an explicit model, the rebar and concrete are discretized into beam and solid elements, respectively. The concrete volume is modeled using 8-node solid hexahedron elements which have three degrees of freedom at each node. The stirrup and longitudinal reinforcements in the concrete are modeled as two-node beam elements using the Hughes–Liu beam element formulation. A coupled algorithm provided by LS-DYNA is applied to simulate the concrete–rebar interaction. The velocity and acceleration of rebar nodes are distributed to related concrete nodes, and then, the two updated variables of the concrete nodes are redistributed to the beam nodes. So, the momentum conservation and the force balance can be achieved, and the rebar can move almost the same way as the concrete.

The background of the impact analysis in Fig. 1 is the Shenzhen landslide, which occurred on 20 December 2015. The landslide destroyed 33 modern buildings, leading to 73 deaths and 17 injuries. This case provides not only the building prototype and the landslide material parameters but also a chance to investigate the failure mechanisms of buildings.

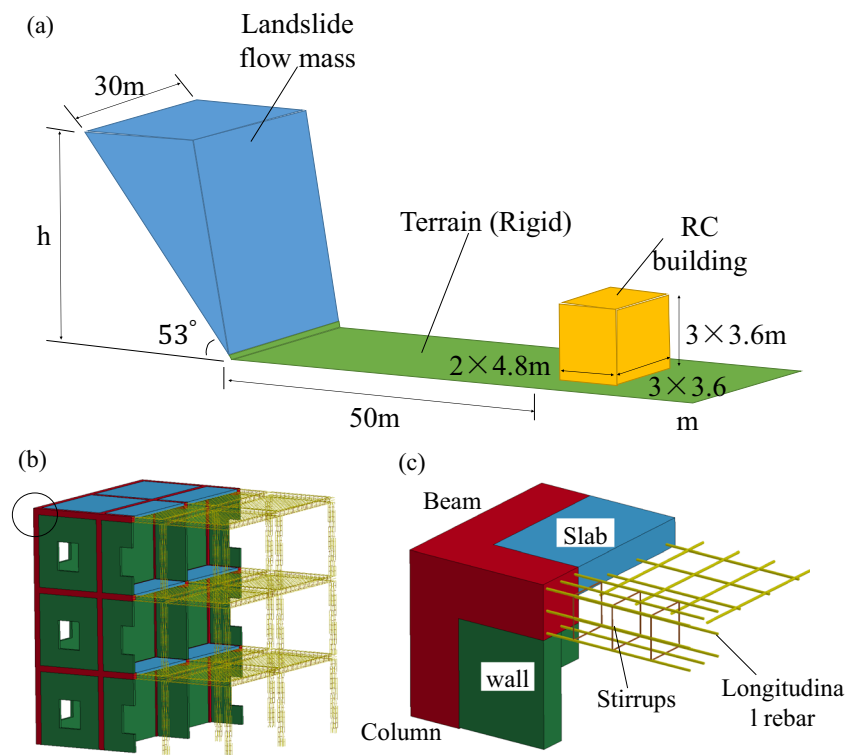


Fig. 1 Finite element model: (a) global model; (b) RC-framed building; and (c) detailed configuration

The modeling of reinforced concrete structures is firstly validated against a single-beam analysis. Then, progressive collapse analysis is conducted on a 2-bay (4.8 m), 3-span (3.6 m), and 3-story (3.6 m) RC-framed structure, which is a typical building structure type. Figure 1 shows the globe numerical model and the RC building details. The relative distance between the landslide mass and the building is 50 m, which is scaled down from the background case. The width of the flow channel is 30 m. The reinforcements of the columns and beams consist of 8@14 longitudinal rebars and 8-mm-diameter hoops placed at 200 mm spacing. The transverse and longitudinal reinforcements of the slab are modeled at 200 mm spacing. The section of the columns and beams is rectangular; 300 mm × 300 mm in dimension. The thickness of the slabs and walls is 150 mm. The window size is 1.2 m × 1.4 m at 0.9 m height from the bottom of the wall. The windows and doors are assumed to have no resistance to the landslide impact and are not modeled.

Material models

The landslide flow mass is simulated as a single-phase frictional soil material (MAT_SOIL_AND_FOAM), which is assumed to be elasto-plastic, and described by the Drucker–Prager yield criterion. This material model has been shown to be able to simulate well landslide dynamics (Kwan et al. 2015; Koo et al. 2017). The deviatoric perfectly plastic yield function, f , is described in terms of the second stress invariant J_2 :

$$f = J_2 - [a_0 + a_1 p + a_2 p^2] \quad (1)$$

where a_0 , a_1 , and a_2 are coefficients and p is the mean stress.

The original Drucker–Prager (D–P) yield criterion can be expressed as:

$$\sqrt{J_2} = A + BI_1 \quad (2)$$

where I_1 is the first invariant of Cauchy stress; J_2 is the second invariant of the deviatoric part of Cauchy stress; and A and B are material coefficients. Since $p = I_1/3$, we can obtain $a_0 = A^2$, $a_1 = 6AB$, and $a_2 = 9B^2$.

Given friction angle ϕ and cohesion c , the corresponding yield function parameters, A and B , in Eq. (2) can be calculated by:

$$A = \frac{2\sqrt{3}c \cos\phi}{(3 + \sin\phi)}, B = \frac{2 \sin\phi}{\sqrt{3}(3 + \sin\phi)} \quad (3)$$

According to Yin et al. (2016), the flow material in the Shenzhen landslide was soft and wet and is considered saturated in this paper. The shear strength parameters of the samples were determined using consolidated quick direct shear test. The minimum undrained shear strength parameters were $\phi = 20^\circ$ and $c = 10$ kPa. In this paper, these parameters are used to reproduce the flow process by assuming an undrained condition during the landslide flow process as the duration of flow and impact is short.

The constitutive material models for reinforcements and concrete need to be determined separately. A three-invariant cap model is

applied to describe the concrete behavior (*MAT_CSCM_CONCRETE). The yield function is expressed by Murray (2007) as:

$$f(J_1, J_2, J_3, \kappa) = J_2 - \mathfrak{R}^2 F_f^2 F_c \quad (4)$$

where F_f is the shear failure surface:

$$F_f(J_1) = \alpha - \lambda \exp^{-\beta J_1} + \theta J_1 \quad (5)$$

The values of α , β , λ , and θ are selected by fitting the model surface obtained from the triaxial compressive tests on plain concrete cylinders. The intersection of the shear surface and the cap is at $J_1 = \kappa$. F_c is the hardening cap:

$$F_c(J_1, \kappa) = 1 - \frac{[J_1 - L(\kappa)][|J_1 - L(\kappa)| + J_1 - L(\kappa)]}{2[X(\kappa) - L(\kappa)]^2} \quad (6)$$

where $L(\kappa)$ is defined as $L(\kappa) = \begin{cases} \kappa & \text{if } \kappa > \kappa_0 \\ \kappa_0 & \text{otherwise} \end{cases}$ and κ_0 is the value of J_1 at the initial intersection before hardening occurs as the cap moves. F_c is equal to unity for $J_1 \leq L(\kappa)$ and elliptical for $J_1 > L(\kappa)$. The intersection of the cap with the J_1 axis is $X(\kappa)$. This value depends on the cap ellipticity ratio R , which is the ratio of the major and minor axes: $X(\kappa) = L(\kappa) + RF_f(L(\kappa))$. \mathfrak{R} , which is calculated based on the Lord angle and experimentally determined values at different pressures, is used to determine the strength of concrete at any state of stress relative to the strength at the triaxial compression state; for example at the triaxial tension state or torsional state. The advantage of this model is that it models the complex behavior of concrete by specifying the unconfined compressive strength only.

An elastic-plastic material model is employed to model the longitudinal steel reinforcements and stirrups. This model is able to properly describe the hardening behavior of steel. HRB400 reinforcing bars are applied. The masonry wall is a more complex component, as it comprises of masonry bricks and mortar. Considering the fact that the wall components always fail in a brittle manner, in this paper, an elastic-perfect-plastic material is utilized considering the strength in tension. The constitutive model parameters for different materials are summarized in Table 1.

In continuum modeling and numerical simulations, erosion techniques are often used to avoid computer overflow. If any element reaches the prescribed failure thresholds, it will be assumed to have no resistance to any loading and then deleted from the calculation. In the present study, the failure criteria of concrete are based on the maximum principal strain provided by the model. A concrete element is deleted when it reaches a maximum principal strain of 0.2. The wall elements are deleted when the plastic strain reaches 0.1. A plastic failure strain of 0.1 is adopted for the reinforcements in concrete. It should be noted that these values are obtained by trial and error. If they are too large, computer overflow and element distortion will still occur. If these values are too small, a large number of elements will be deleted, which is not reasonable and may lead to numerical instability. Using this erosion algorithm, the progressive collapse process of buildings can be observed clearly.

Boundary conditions, loadings, and contact interfaces

The foundation of the building is not considered in the numerical model, and fixed boundary conditions are assigned for the bottom

Table 1 Constitutive model parameters

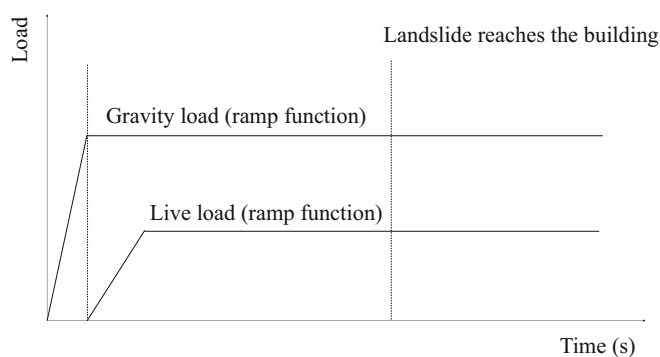
Parameters	Landslide soil	Concrete	Steel reinforcement	Infill wall
Bulk density, ρ (kg/m ³)	2000	2400	7850	1800
Elastic modulus, E (MPa)	20	23,000	200,000	5900
Poisson's ratio, ν	0.3	0.15	0.30	0.15
Undrained friction angle, ϕ (°)	20	–	–	–
Undrained cohesion, c (kPa)	10	–	–	–
Unconfined compressive strength (MPa)	–	20.1	–	–
Yield stress (MPa)	–	–	400	0.53
Ultimate stress (MPa)	–	–	540	–
Failure strain	–	0.20	0.10	0.10

nodes of the columns and walls. This implies that only the superstructure can be affected by the landslide impact. All the degrees of freedom of the landslide nodes at the bottom are fixed. Slide boundary conditions are applied on the nodes at the sides of the landslide mass. Both the dead loads (gravity) and live loads are considered. According to the load specifications for the design of building structures (MOHURD 2012), a uniformly distributed load of 2 kN/m² is imposed on the top surface of the slab and roof. The gravity load is applied as a ramp loading function and maintained constant once it reaches the peak gravity load level. Subsequently, the live load is applied in a similar ramp function (Fig. 2).

The Coulomb frictional rule and a penalty method are applied at the landslide–terrain interface and the landslide–barrier interface. The penalty method places an imaginary normal interface spring at the contact surface. The contact force is calculated based on the interface stiffness and the penetration depth (Hallquist 2006). A penalty factor f_{si} (default = 0.1) is used to scale the estimated stiffness k_{si} . For a solid element, the scaled stiffness is:

$$k_{si} = \frac{f_{si} K_i A_i^2}{V_i} \quad (7)$$

where K_i is the bulk modulus; A_i is the face area of the element; and V_i is the volume of the element. The friction coefficient, μ , at the landslide–terrain interface is taken as 0.30, which is obtained by trial and error to get a predetermined impact velocity. The friction coefficient at the landslide–barrier interface is set to 0.36, which is given by $\mu = \tan \phi$.

**Fig. 2** Loading stage in the numerical model

Progressive building collapse processes

Before conducting the impact analyses, validation of the modeling method for the reinforced concrete components has been performed. The three-point bending test on a typical RC beam is simulated to validate the method. The validation case is described in detail in the Appendix.

In this paper, three impact energy cases, namely low-, moderate-, and high-impact intensity cases with three frontal impact velocities of 4.8, 6.8, and 8.8 m/s, respectively, are carried out. In order to generate a series of landslides with different levels of kinetic energy, only the height of slope is varied and all other conditions are identical with each other. The slope heights for the three levels of kinetic energy are 28.3, 30.2, and 32.2 m, respectively. The progressive development of building damage state, thus, can be observed clearly and verified with each other conveniently.

The impact processes of these three impact cases are shown in Figs. 3, 4 and 5. Figure 3 shows the final stage of the building impacted by a landslide in the low-impact intensity case. In this case, only the frontal wall failure is observed. The frontal walls are destroyed, first, due to its low out-of-plane flexural capacity; then, the landslide material flows into the building, reaching one half bay of the building. The primary structural components are not damaged because of the low kinetic energy of the landslide in this case. A building damaged in this manner was observed in the Shenzhen landslide, as shown in Fig. 6a. This building was located at the distal end of the landslide; the kinetic energy of the landslide front was too small to cause structural damage.

Figure 4 shows the snapshots of the building damage observed in the moderate-impact intensity case. After the failure of the frontal walls, two corner columns are damaged, followed by the destruction of the side walls behind the corner columns. The two middle columns still bear the superstructure loads. After the destruction of the frontal walls, the material flows into the building and destroys the inner walls in the 2nd row (Fig. 4b). However, the material does not reach the corner columns in the 2nd row due to the fact that the columns have higher resistance than the brick walls and part of the kinetic energy of the flow material has been absorbed by the 1st row corner columns. After the failure of the columns, the superstructure loads are arrested by the beam and infill wall system above the failed column, avoiding collapse of the building. This damage state of building was observed in the Zhouqu debris flow (Fig. 6b). Overall, the kinetic energy of the landslide in this moderate-impact intensity case is not sufficient to

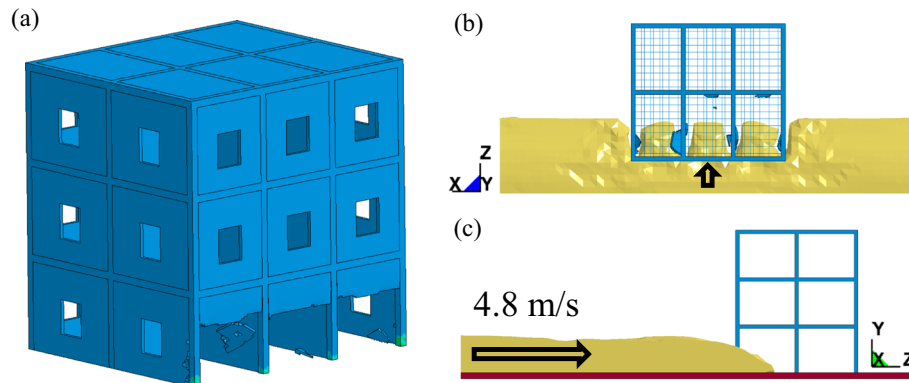


Fig. 3 Snapshots of the frontal wall failure in the low-impact intensity case: (a) oblique view; (b) top view; and (c) side view

cause the collapse of the building and only local damage occurs. The failure mechanism of the two corner columns will be discussed later.

Figure 5 shows the progressive collapse process of the building in the high-impact intensity case. Unlike the situation in the moderate-impact case, following the failure of the corner columns, the two middle columns are also damaged during the initial impact. Then, the landslide debris marches forward and destroys the walls behind the damaged columns. Because of the larger kinetic energy, the flow material reaches the columns in the 2nd row, destroying the two corner columns in the 2nd row first and the two middle columns in the 2nd row subsequently, since the flow material reaches the corner columns in the 2nd row earlier (Fig. 5g). Although the strength of the corner and middle columns is the same, the failure times are different. This is caused by the different failure mechanisms and conditions of the flowing material. After this moment, only the columns in the 3rd row remain, which are not sufficient to bear the superstructure loads. The whole building starts to fall forward, and damage initiates on the top of the columns in the 3rd row. Finally, the whole building collapses. This state of building damage was observed in the Shenzhen landslide (Fig. 6d). This building was located at the near end, and its bottom floor was totally destroyed, followed by the collapse of the upper floors.

The building collapse is induced by the progressive failure of columns, which are the main components to bear the vertical load for the RC-framed building. Figure 7 shows the vertical loading transfer in the columns. In Fig. 7a, after the initial impact, the axial forces in the 1st row columns start to increase and the corner columns fail at 5.5 s with an axial force of 300 kN. After that moment, the axial forces in the middle columns increase suddenly to 400 kN, and the failure of the middle columns is observed at 5.6 s. The axial force, then, transfers to the columns in the 2nd row, quickly increasing from 100 to 400 kN, followed by the gradual increase to 700 kN from 5.7 to 6.4 s. This stage corresponds to the failure of the side walls in the 1st bay. At 6.5 s, the flow material reaches the corner columns in the 2nd row, and failure occurs. The axial force, then, transfers to the middle columns in the 2nd row with a dramatic increase from 700 to 1700 kN, and the middle columns fail. The above-mentioned progressive vertical loading transfer in the high-impact case can also be partially observed in the moderate-impact intensity case (Fig. 7b).

Failure mechanisms of building components

The collapse of the RC-framed building is induced by failure of the vertical bearing components, i.e., the columns. As mentioned previously, the corner columns are the first bearing components destroyed by the landslide. Figure 8 shows the time histories of the earth pressure behind the corner and middle columns in different

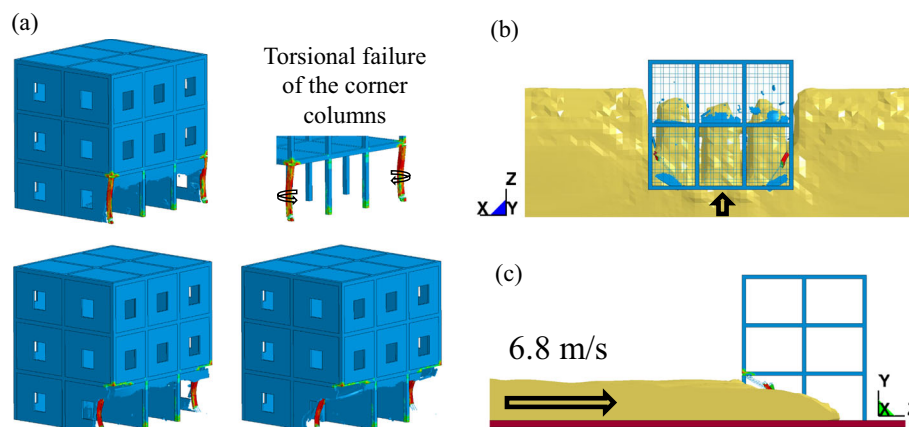


Fig. 4 Snapshots of impact process in the moderate-impact intensity case: (a) oblique view; (b) top view; and (c) side view

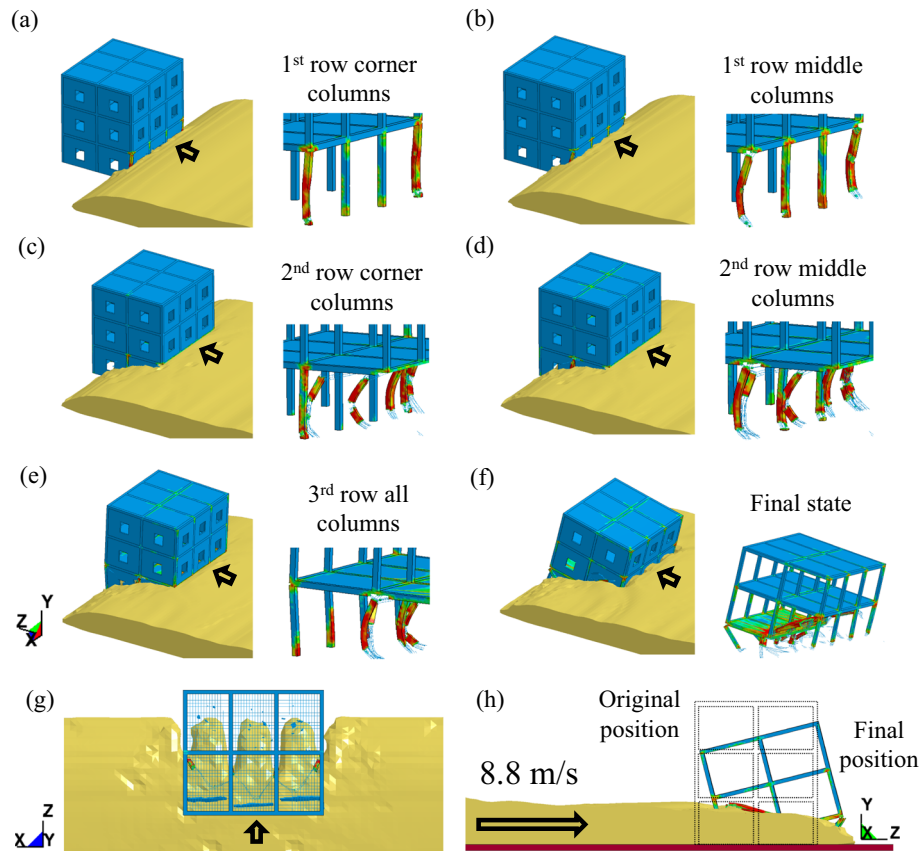


Fig. 5 Snapshots of progressive building collapse in the high-impact intensity case: (a–f) oblique view; (g) top view; and (h) side view

impact cases. For the corner columns, in all three impact cases, there is a pressure difference among the left, front, and right sides of the corner columns due to the different flow conditions. The highest peak earth pressures occur in the front of the corner columns, from a strong interaction between the columns and the flowing landslide material. The smaller peak earth pressures on the left and right sides of the corner columns reflect two facts. First, the landslide material can flow through the open area on one side. Second, the frontal walls on another side almost have no resistance under the out-of-plane loading induced by the landslide and can be suddenly destroyed. This leads to a weaker interaction mechanism and, hence, a smaller peak earth pressure. Similarly, the highest peak earth pressure occurs in the front of the middle column. However, the earth pressures on the left and right sides of the middle column are almost the same due to the similar flow condition.

Because of the pressure difference on the corner columns, torques are produced on the corner columns (Fig. 9). The ultimate torque is about 25 kNm for the high- and moderate-impact intensity cases, at which the corner columns are destroyed. In the low-impact intensity case, in which the corner columns do not fail, the maximum torque is about 12 kNm. A complex flexural–torsional failure mechanism is observed for the failed corner columns, which leads to a lower ultimate bending moment than the pure bending failure of the middle columns. Figure 10 shows the time histories of the bending moment on the bottom of the columns. In

the high-impact intensity case, the ultimate bending moment in the failed 1st row corner column is about 50 kNm, which is lower than that in the failed 1st row middle columns (i.e., 75 kNm in Fig. 10a). The ultimate bending moments are about 90 kNm for the columns in the 2nd row (Fig. 10b). This slight increase of the ultimate bending moment is caused by the increased axial force in the column.

In the moderate-impact intensity case, the ultimate bending moment in the failed 1st row corner column is also 50 kNm. For the middle column, although the peak bending moment is still large (Fig. 10c), a plastic zone only appears at the bottom, which is a fixed end directly impacted by the landslide. After this initial impact, the walls behind the middle columns do not collapse due to the lower impact energy. A plastic hinge does not develop at the top of the column. In this way, the middle columns do not experience bending failure. In the low-impact intensity case, no structural components are destroyed as the bending moments on the columns are small (Fig. 10d).

From the discussion in the previous texts, it can be concluded that the interaction mechanism and the failure mechanism of the RC columns are well captured by the impact analyses. The plastic hinge theory can well explain the failure mode of the columns. The failure of the building components occurs at the same time of the peak pressure in this study. If the impacted components survive from the initial impact of landslide, a safer condition would be achieved due to the quick drop of the impact pressure.



http://news.cri.cn/gb/27824/2010/08/10/782s2950188_13.htm

Fig. 6 Building damage states observed in Shenzhen landslide and Zhouqu debris flow

Vulnerability of buildings

To estimate the vulnerability of buildings to landslides or debris flows, the damage state of the building and the landslide intensity need to be determined. To accurately evaluate the building damage state, it is necessary to establish a classification system based on the specified damage scenario and failure mechanisms. Leone et al. (1996) provided a sample of levels of damage to buildings. Vamvatsikos et al. (2010) identified building damage based on collapse mechanisms observed in field studies. Hu et al. (2012) proposed a classification scheme based on a classification system of earthquake damage to buildings. Mavrouli et al. (2014) also defined five

damage states considering hierarchies of structural components. Kang and Kim (2016) applied the classification scheme proposed by Leone et al. (1996) and Hu et al. (2012) to determine the damage degree of buildings. However, the hierarchies of the damage state of buildings are not clear as they are established according to expert experience on building damage state. Moreover, the description of the level of damage is not specific and not unified in the existing systems, which impedes their application in landslide risk analysis.

In this paper, a five-class classification system for RC buildings is proposed (see Table 2) on the basis of the work done by the above-mentioned researchers considering the impact analysis

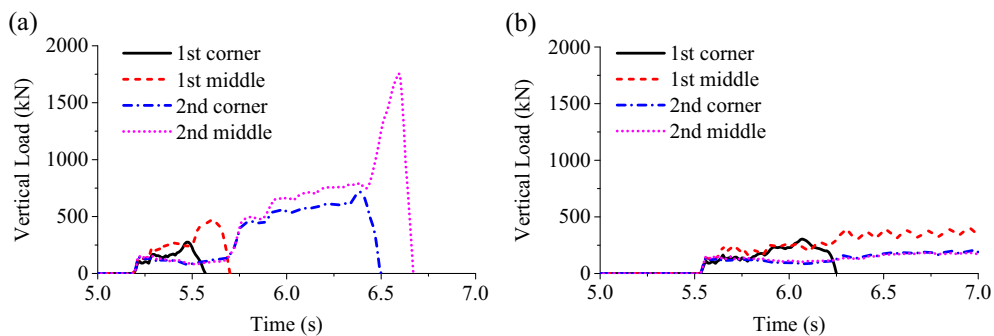


Fig. 7 Vertical loading evolution in the columns: (a) high-impact intensity case and (b) moderate-impact intensity case

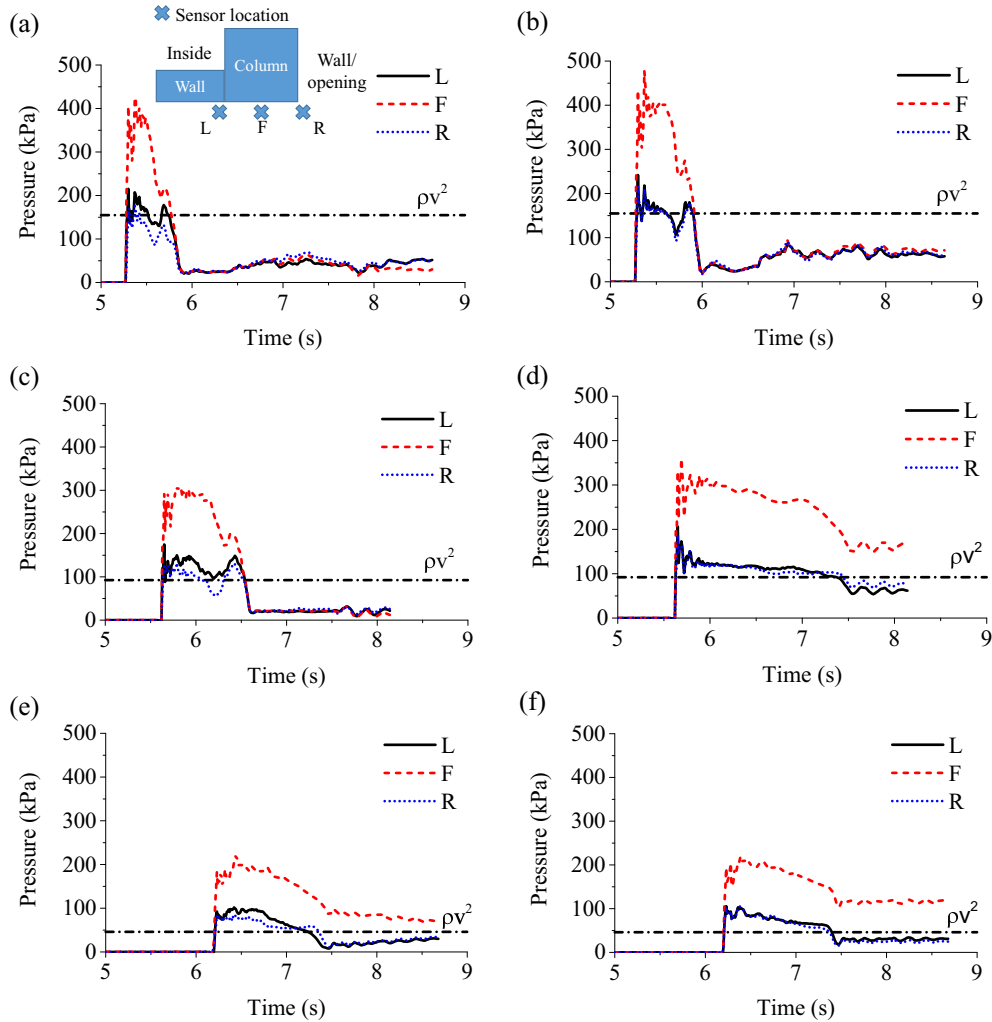


Fig. 8 Pressure time histories on the columns: (a) corner columns in the high-impact intensity case; (b) middle columns in the high-impact intensity case; (c) corner columns in the moderate-impact intensity case; (d) middle columns in the moderate-impact intensity case; (e) corner columns in the low-impact intensity case; (f) middle columns in the low-impact intensity case

results. The hierarchy of the damage state can be established more solidly as the progressive failure process and failure mechanisms of building components have been fully explored. The vulnerability value here is expressed as the damage degree of building and determined based on Leone et al. (1996) and Kang and Kim (2016). It is worth noting that, under the framework of quantitative risk assessment, the risk may be expressed as the annual monetary loss per area unit (Corominas et al. 2014). Hence, the physical damage degree can also be correlated to the repair cost by calculating the repair cost of the damaged components directly as the damage scenario has been specified for each damage state. The proposed classification system, thus, can be applied to the evaluation of the damage state of specified RC buildings.

To predict the building vulnerability to landslide, the landslide intensity is also required. The landslide intensity can be expressed by flow depth, impact pressure, or impact velocity. Among them, impact pressure is an essential indicator of landslide intensity. In the above-mentioned three impact cases, the maximum-impact pressures occur at the bottom of the columns and are almost the same for the corner and middle columns, approximately 477, 323, and 222 kPa in the high-, moderate-, and low-impact intensity

cases, respectively. The hydrodynamic model, which is most commonly used to estimate the maximum pressure, is expressed as:

$$p_{\max} = \alpha \rho v^2 \quad (8)$$

where p_{\max} is maximum impact pressure; α is a dynamic empirical factor; ρ is the density of debris; and v is the frontal flow velocity.

In this paper, the α values for the three impact cases are deduced in Table 3. The deduced Froude number (Fr) values are 1.45, 1.18, and 0.89 for the high-, moderate-, and low-impact intensity case, respectively. The α value for each case is not identical but increases with the decrease of Fr. In the literature, the hydrodynamic model has been investigated by many researchers (e.g., Lichtenhahn 1973; Hungr et al. 1984; Armanini 1997; Hübl and Holzinger 2003; Hübl et al. 2009; Canelli et al. 2012; Cui et al. 2015). Variations in α were observed due to the following several factors: boulder effect (Wu et al. 1993) or large particle effect, inhomogeneity of the fluid, and gravitation effect. This model is developed based on the global momentum balance to a control volume of incompressible flow; hence, the impact pressure in this model is the average pressure induced (Lo 2000). However, the obtained pressure here is a local value, and the compressible characteristic of the earth flow cannot be

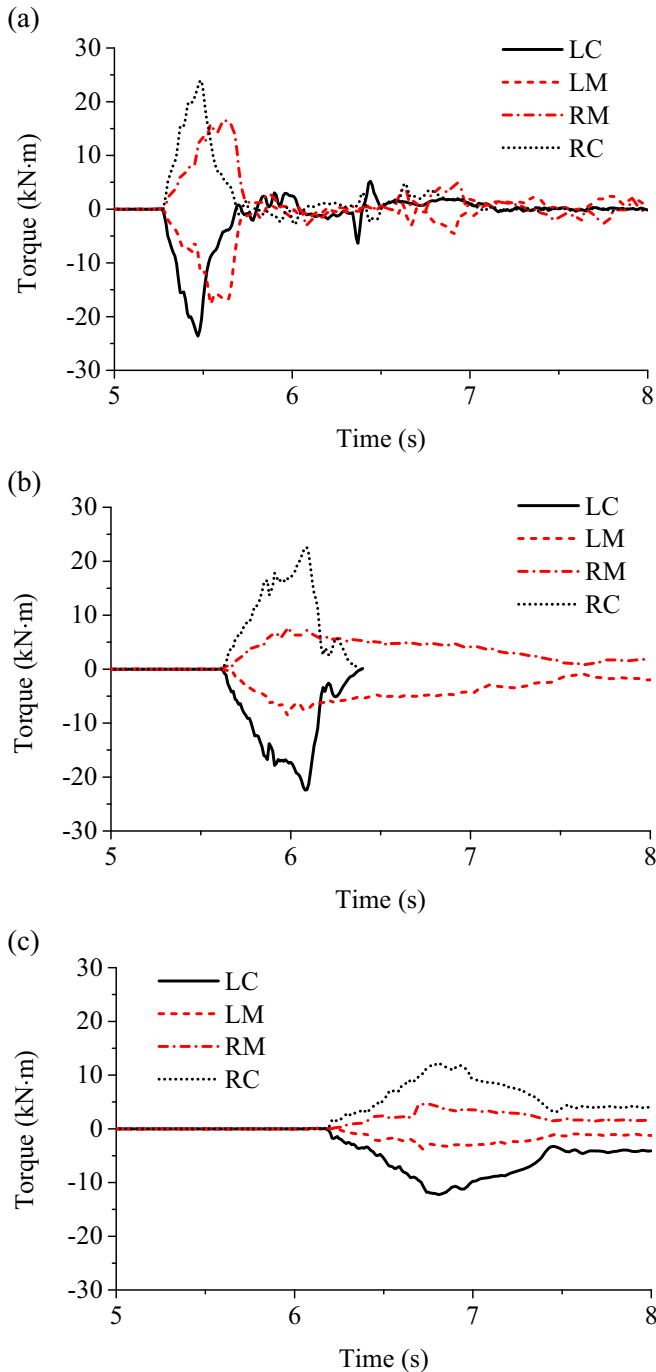


Fig. 9 Torques on the 1st row columns: (a) high-impact intensity case; (b) moderate-impact intensity case; (c) low-impact intensity case (notes: L, left; R, right; C, corner; M, middle)

considered by this model. Moreover, it is commonly accepted that the impact pressure consists of both hydrostatic and hydrodynamic parts. The gravitational component is not involved in the hydrodynamic model. That is why Hübl and Holzinger (2003) proposed a power model considering both components:

$$P_{\max} = (aFr^b)\rho v^2 \quad (9)$$

$$Fr = v/\sqrt{gh} \quad (10)$$

in which the relationship between Fr and the dynamic empirical factor α is established by data fitting with two coefficients $a = 4.5$ and $b = -1.2$. The calculated Fr values and dynamic empirical factors for the three impact cases follow well the established relationship given in Hübl and Holzinger (2003). In Fig. 11, the predicted impact pressure values based on Eq. (9) are also very close to the simulated results. These may be attributed to the scale-free relationship of this model. Both the dynamic/inertia component (v) and the static/gravitational component (h) are involved in the power model. Therefore, the power model can be applied to predict the maximum impact pressure.

After reaching the maximum pressure, if the impacted column is destroyed, the earth pressure will decrease quickly and finally reach the static earth pressure. Figure 8a,b shows that the static earth pressures for the corner columns are smaller than those for the middle columns in the high-impact intensity case. This is due to the different failure mechanisms of the columns. The higher the resistance of the columns is, the more kinetic energy of the landslide will be absorbed, leading to a lower flow velocity. In this way, after the failure of the middle columns, the material flows slower and the earth pressure cannot be easily released. The above-mentioned phenomenon can be more easily observed in the moderate-impact intensity case (Fig. 8c,d). The static earth pressures behind the middle columns are much higher than those behind the corner columns due to the fact that the middle columns are not destroyed. Figure 8e,f shows the static earth pressure in the low-impact intensity case. As only the frontal walls fail, the slight difference on the static earth pressures behind the corner and middle columns is caused by the better flow condition near the corner columns.

For a building under a given impact intensity of landslide, the responses of the building components can be obtained by combining the failure mechanisms with an impact pressure model. The resistance of each structure component can also be obtained analytically based on the identified failure mechanisms and material properties; namely, the out-of-plane flexural failure in frontal walls (slightly damage state), the bending failure of columns (moderately damage state), and the resistance of the beam and infill wall system above the damaged columns to the partial collapse (heavily damage state). The completely damage state can be evaluated by a threshold of landslide intensity, e.g., 9 m/s in this paper. Kang and Kim (2016) also obtained a threshold velocity of 9.4 m/s to reach vulnerability factor $V = 1.0$ for RC-framed buildings. The vulnerability of the buildings to a landslide or debris flow, thus, can be assessed. Note that the physical vulnerability of a building depends on both the building characteristics and the impact load. A single parameter (e.g., impact pressure given in Hu et al. 2012) is insufficient to indicate the building damage state.

Summary and conclusions

A significant research gap exists in assessing the vulnerability of buildings to landslides. The understanding of the failure mechanism of buildings impacted by landslides can provide a solid basis for robust building design and building vulnerability assessment. In this paper, an explicit integration program has been utilized to analyze the response of typical RC-framed buildings impacted by landslides. Three impact cases with different frontal impact velocities, namely, low-, moderate-, and high-impact intensity cases,

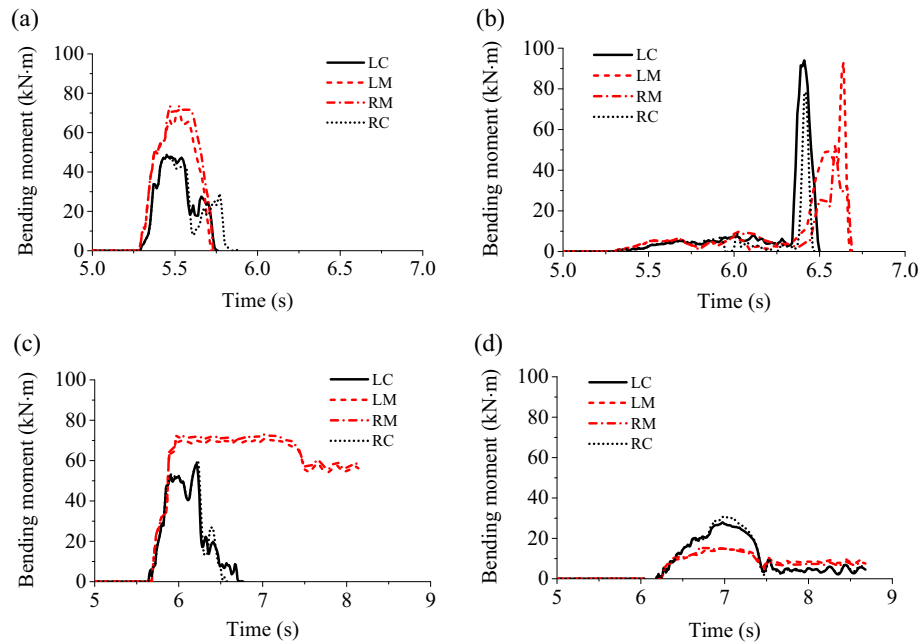


Fig. 10 Bending moment on the bottom of the columns: (a) 1st row columns in the high-impact intensity case; (b) 2nd row columns in the high-impact intensity case; (c) 1st row columns in the moderate-impact intensity case; (d) 1st row columns in the low-impact intensity case (notes: L, left; R, right; C, corner; M, middle)

were evaluated, and progressive failure of the building was observed. The key findings are summarized as follows:

1. The frontal walls in the ground floor are the first damaged component due to their low out-of-plane flexural capacity. The landslide material, then, flows into the building and destroys the remaining components.
2. If the impact energy of a landslide is large enough, the structural components of the building on the ground floor can be destroyed in the sequence of frontal walls, 1st row corner columns, 1st row middle columns, walls behind the damaged columns, and, finally, the columns in the next row. The columns are critical structural components, and the building collapse is caused by the progressive failure of the columns. The whole building will collapse when the remaining columns cannot resist the superstructure loads.
3. The beam and infill wall system provides resistance to the vertical loads above the failed columns and arrests partial

Table 2 Classification of damage states for RC buildings impacted by landslides and debris flows

Damage state	Damage description	Case histories	Damage degree (0 means no damage and 1.0 means totally damaged)
Completely	Serious damage of the majority of the structural components (i.e., columns), leading to collapse of the whole building or translation of remaining building	High-impact intensity case; Fig. 6d for total collapse and Fig. 6e,f for translational movement (observed in Shenzhen landslide)	0.7–1.0
Heavily	Serious damage or collapse of several structural components, leading to partial collapse of the building	Fig. 6c (observed in Zhouqu debris flow)	0.5–0.7
Moderately	Serious damage or collapse of several structural components (i.e., columns) without collapse of the building	Moderate-impact intensity case; Fig. 6b (observed in Zhouqu debris flow)	0.3–0.5
Slightly	Cracks occur on the nonbearing walls or collapse of the external walls directly impacted by the debris; no significant damage of the primary bearing components (columns and beams)	Low impact intensity case; Fig. 6a (observed in Shenzhen landslide)	0.1–0.3
Very slightly	Only the non-structural components are damaged (windows and doors); no significant damage of the primary (columns and beams) and secondary structural components (slabs and infill walls)	Mavrouli et al. (2014)	0–0.1

Table 3 Comparison of frontal Fr and α values

Impact intensity	Velocity (m/s)	Flow depth (m)	Froude number, Fr	Dynamic pressure coefficient, α
High	8.8	3.7	1.45	3.08
Moderate	6.8	3.3	1.18	3.50
Low	4.8	2.9	0.89	4.79

- collapse of the building. The ability of this cantilever system to prevent subsequent collapse depends on the bending capacity of the beam.
- Bending failure is the most common column failure mode, which usually occurs near the time of the peak impact pressure. The side walls behind the columns provide a lateral constrain and enhance the flexural capacity of the column due to the higher in-plane rigidity of walls. Torsional-flexural failure can occur on the corner columns when the flow conditions on both sides of the columns are not symmetrical.
 - The five-class classification system proposed in this paper well represents the progressive development of building damage as the progressive failure process of a typical RC building is fully explored. The clear hierarchy of damage degree and the physical description of damage state provide more accurate evaluation of the damage state of buildings, moving the scientific knowledge on building vulnerability assessment forward. The vulnerability of the buildings to a landslide or debris flow can be assessed quantitatively based on the identified failure process, failure mechanisms, and an impact pressure estimation model, promoting the development of quantitative risk assessment of landslides.
 - It is worth noting that the impact cases in this paper are deterministic analyses. The fragility analysis, which involves the inherent uncertainties on the characteristics of both the landslide (e.g., Orr 2017 and Xiao et al. 2017) and the building, has not been developed due to computational efficiency issues. Nevertheless, the applied method provides a powerful tool to investigate the key factors on building

vulnerability, which would be helpful for developing fragility functions. Reliability-based vulnerability models, considering variations on the material property and the impact loading, will be developed using computationally less-demanding analyses.

Acknowledgments

The authors acknowledge the support from the Research Grants Council of the Hong Kong SAR (Nos. T22-603/15N and C6012-15G).

Appendix-model verification: beam analysis

In order to validate the applied numerical model, a typical RC beam, which is commonly used in China, is selected to conduct the three-point bending test simulation (Zeng et al. 2015). Two rigid cylindrical supports are set to support the beam. A concentrated load is imposed on the middle span of the beam in a ramp function and monotonically increased until failure. The failure process is analyzed, and the simulated cracking moment of concrete, ultimate bending moment of the beam, and time history of axial stress in the rebar are compared with the analytical results calculated based on the limit state theory for reinforced concrete structure design. The material parameters for the beam model are identical to those for the building model in Table 1. The cracking moment can be calculated based on the specification for the design of concrete structure (MOHURD 2010): $M_{Cr} = f_{tk} W_o = 7$ MPa, where f_{tk} is the concrete tensile characteristic strength and W_o is the resistance moment of the equivalent cross-section. For the cross-section at the middle span, the stress in the rebar before cracking is calculated as $\sigma_{cr-b} = E_s f_{tk} / E_c = 14$ MPa, where E_s and E_c are the Young’s modulus of rebar and concrete, respectively. After cracking, the stress in the rebar is expressed as $\sigma_{cr-a} = E_s f_{tk} / E_c + f_{tk} A_c / A_s = 154$ MPa, where A_c and A_s are the areas of tensile concrete and tensile rebar, respectively. Besides, as shown in Fig. 12, the ultimate bending moment of the beam can be calculated based on force equilibrium (Eq. (11)) and moment equilibrium (Eq. (12)):

$$f_y A_s = \alpha_1 f_{ck} b x + f'_y A'_s \tag{11}$$

$$M_u = \alpha_1 f_{ck} b x \times \left(h_o - \frac{x}{2} \right) + f'_y A'_s \left(h_o - a'_s \right) \tag{12}$$

where f_y and f'_y are the tensile and compressive stresses of the longitudinal reinforcement, respectively; A_s and A'_s are the areas of tensile and compressive longitudinal reinforcement,

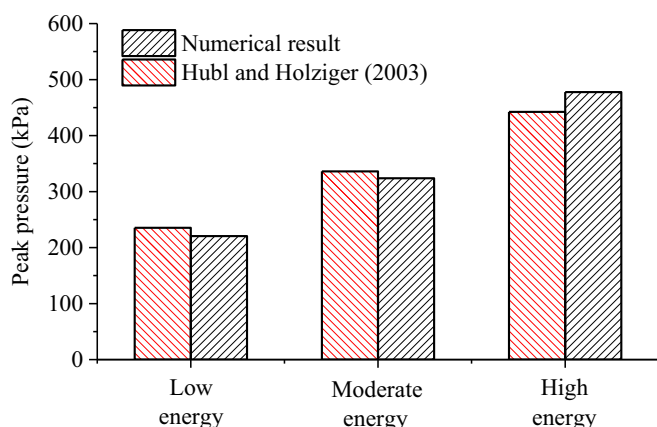


Fig. 11 Comparison between numerical results and the power models for the maximum-impact pressure

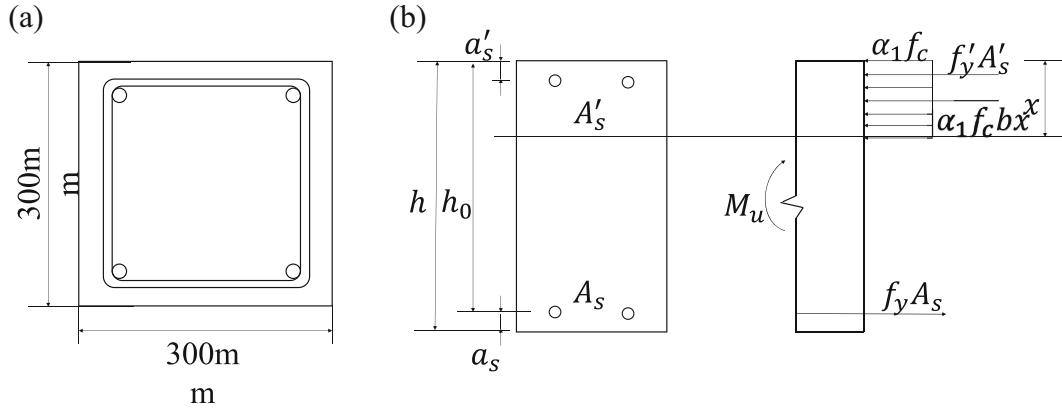


Fig. 12 (a) Cross-section and (b) diagrams for calculating bearing capacity of beam

respectively; α_1 is a coefficient of concrete grade; f_{ck} is the concrete compressive characteristic strength; b is the width of column section; x is the compression height; and h_0 is the effective height of the cross-section. If $x < a_s$, the compressive stress of the rebar does not reach f_y ; so, the ultimate bending moment can be calculated by assuming $x = a_s$ and taking a moment to the centroid of compressive rebar; $M_u = f_y A_s (h_0 - a_s) = 40$ kNm.

Snapshots of typical beam failure process from the numerical analysis are shown in Fig. 13. The development and distribution of cracks are described by the contours of the plastic strain. At 0.10 s, the cracking moment is reached, and, then, cracks occur in the

tensile zone. Besides, the stress of the tensile rebar experiences a rapid increase at the crack point, from 16 to 157 MPa (Fig. 14). After cracking, the stresses of the tensile reinforcement and compressive concrete increase with the applied pressure, and, finally, the beam

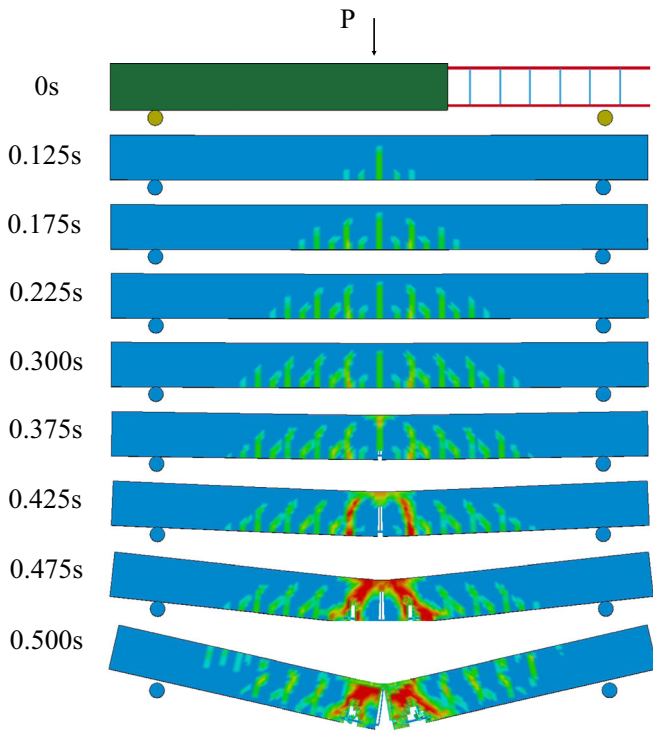


Fig. 13 Snapshots of beam failure process: contours of plastic strain

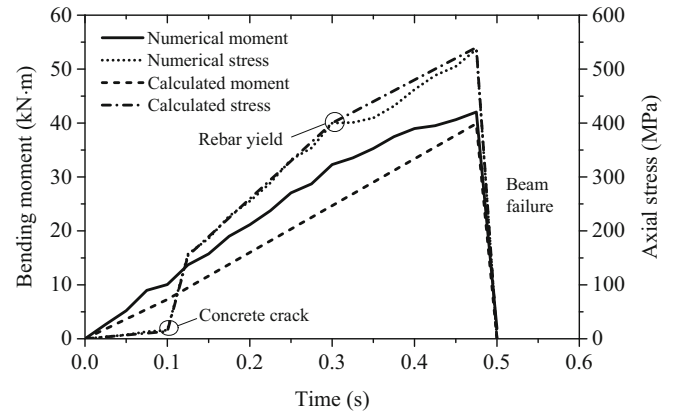


Fig. 14 Time histories of bending moment and axial stress of the reinforcement at the middle span

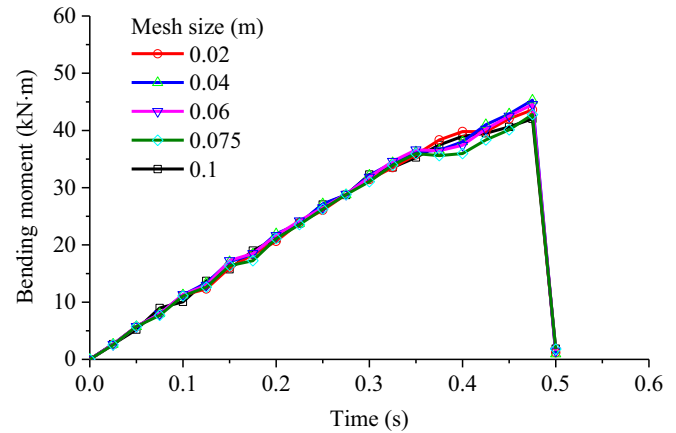


Fig. 15 Time histories of bending moment at the middle span for different concrete element sizes

reaches the ultimate bending moment state. The numerical model reflects well the typical beam failure process, and the simulated results are very close to those from the static analysis.

To consider the mesh size effect, the same three-point bending tests are simulated using different element sizes of the concrete beam. The time histories of bending moment at the middle section are compared in Fig. 15. The different element sizes almost produce the same results. Considering that the stability of the explicit integration scheme is determined by the time step, a smaller element size allows smaller time step to ensure a stable analysis and, thus, requires significantly longer computing time. So, a mesh size of 0.075 m is applied in the impact analysis.

References

- Akbas SO, Blahut J, Sterlacchini S (2009) Critical assessment of existing physical vulnerability estimation approaches for debris flows. In: Malet JP, Remaitre A, Bogaard T (eds) Proceedings of landslide processes: from geomorphologic mapping to dynamic modelling. Strasburg, France, 6–7 February 2009, pp 229–233
- Almusallam TH, Mendis P, Ngo T, Elsanadedy HM, Abbas H, Alsayed SH, Al-Salloum YA, Alhaddad MS (2010) Progressive collapse analysis of a typical RC building of Riyadh. IMPLAST 2010—SEM Fall Conference, University of Rhode Island, USA
- Armanini A (1997) On the dynamic impact of debris flows. Recent developments on debris flows. In: Lecture Notes in Earth Sciences. Springer, Berlin, pp 208–226
- Canelli L, Ferrero AM, Migliazza M, Segalini A (2012) Debris flow risk mitigation by the means of rigid and flexible barriers—experimental tests and impact analysis. *Nat Hazard Earth Syst* 12(5):1693–1699
- Corominas J, van Westen C, Frattini P, Cascini L, Malet JP, Fotopoulou S, Catani F, Van Den Eeckhaut M, Mavrouli O, Agliardi F, Pitilakis K, Winter MG, Pastor M, Ferlisi S, Tofani V, Hervàs J, Smith JT (2014) Recommendations for the quantitative analysis of landslide risk. *B Eng Geol Environ* 73(2):209–263
- Cui P, Zeng C, Lei Y (2015) Experimental analysis on the impact force of viscous debris flow. *Earth Surf Process Landf* 40(12):1644–1655
- Eidsvig UMK, Papathoma-Köhle M, Du J, Glade T, Vangelsten BV (2014) Quantification of model uncertainty in debris flow vulnerability assessment. *Eng Geol* 181:15–26
- Elsanadedy HM, Almusallam TH, Alharbi YR, Al-Salloum YA, Abbas H (2014) Progressive collapse potential of a typical steel building due to blast attacks. *J Constr Steel Res* 101:143–157
- Faella C, Nigro E (2003a) Dynamic impact of the debris flows on the constructions during the hydrogeological disaster in Campania—1998: failure mechanical models and evaluation of the impact velocity. In Proc. of the Int. Conf. on “Fast slope movements—prediction and prevention for risk mitigation”, Napoli, May 11–13, 2003, pp 179–186 (in Italy)
- Faella C, Nigro E (2003b) Dynamic impact of the debris flows on the constructions during the hydrogeological disaster in Campania—1998: description and analysis of the damages. In Proc. of the Int. Conf. on “Fast slope movements—prediction and prevention for risk mitigation”, Napoli, May 11–13, 2003, pp 187–193 (in Italy)
- Federico F, Amoroso A (2008) Simulation of mechanical effects due to the impact of fluid-like debris flows on structures. *Ital J Eng Geol Environ* 1:5–24
- Fotopoulou SD, Pitilakis KD (2013) Vulnerability assessment of reinforced concrete buildings subjected to seismically triggered slow-moving earth slides. *Landslides* 10(5):563–582
- Fuchs S, Heiss K, Hübl J (2007) Towards an empirical vulnerability function for use in debris flow risk assessment. *Nat Hazard Earth Syst* 7(5):495–506
- Hallquist JO (2006) LS-DYNA theory manual. Version 971. Software Technology Corporation, Livermore
- Hu KH, Cui P, Zhang JQ (2012) Characteristics of damage to buildings by debris flows on 7 August 2010 in Zhouqu, Western China. *Nat Hazard Earth Syst* 12(7):2209–2217
- Hübl J, Holzinger G (2003) Entwicklung von Grundlagen zur Dimensionierung kronenoffener Bauwerke für die Geschiebewartung in Wildbächen: Kleinmaßstäbliche Modellversuche zur Wirkung von Murbrechern [Development of design basis for crest open structures for debris flow management in torrents: miniaturized tests for the efficiency estimation of debris flow breakers]. WLS report 50 band 3, Im Auftrag des BMLFUW VC 7a. University of Natural Resources and Applied Life Sciences, Vienna (in German)
- Hübl J, Suda J, Proske D, Kaitna R, Scheidl C (2009) Debris flow impact estimation. In Proceedings of the 11th International Symposium on Water Management and Hydraulic Engineering, Ohrid, Macedonia, pp 1–5
- Hungr O, Morgan GC, Kellerhals R (1984) Quantitative analysis of debris torrent hazards for design of remedial measures. *Can Geotech J* 21(4):663–677
- Jakob M, Stein D, Ulmi M (2012) Vulnerability of buildings to debris flow impact. *Nat Hazards* 60(2):241–261
- Kang HS, Kim YT (2016) The physical vulnerability of different types of building structure to debris flow events. *Nat Hazards* 80(3):1475–1493
- Koo RCH, Kwan JS, Lam C, Goodwin GR, Choi C, Ng CWW, Yiu J, Ho KKS, Pun WK (2017) Back-analysis of geophysical flows using 3-dimensional runout model. *Can Geotech J* 55(8):1081–1094
- Kwan JSH, Koo RCH, Ng CWW (2015) Landslide mobility analysis for design of multiple debris-resisting barriers. *Can Geotech J* 52(9):1345–1359
- Leone F, Asté JP, Leroi E (1996) Vulnerability assessment of elements exposed to mass-movement: working toward a better risk perception. In: Senneset K (ed) VII International Symposium on Landslide. A.A. Balkema, Trondheim, Norway, 17–21 June 1996, pp 263–269
- Li Z, Nadim F, Huang H, Uzielli M, Lacasse S (2010) Quantitative vulnerability estimation for scenario-based landslide hazards. *Landslides* 7(2):125–134
- Lichtenhahn C (1973) Die Berechnung von Sperren in Beton und Eisenbeton. Kolloquium on Torrent Dams ODC 384.3. Mitteilungsge der Forstlichen Bundes-Versuchsanstalt, pp 91–127
- Lin F, Ji H, Li Y, Zuo Z, Gu X, Li Y (2014) Prediction of ground motion due to the collapse of a large-scale cooling tower under strong earthquakes. *Soil Dyn Earthq Eng* 65:43–54
- Lo DOK (2000) Review of natural terrain landslide debris-resisting barrier design. Special project report no. SPR 1/2000 (GEO report no. 104), Geotechnical Engineering Office of the Civil Engineering and Development Department, HKSAR
- Lo WC, Tsao TC, Hsu CH (2012) Building vulnerability to debris flows in Taiwan: a preliminary study. *Nat Hazards* 64(3):2107–2128
- Mavrouli O, Corominas J (2010a) Vulnerability of simple reinforced concrete buildings to damage by rock falls. *Landslides* 7(2):169–180
- Mavrouli O, Corominas J (2010b) Rockfall vulnerability assessment for reinforced concrete buildings. *Nat Hazard Earth Syst* 10(10):2055–2066
- Mavrouli O, Fotopoulou S, Pitilakis K, Zuccaro G, Corominas J, Santo A, Cacace F, De Gregorio D, Di Crescenzo G, Foerster E, Ulrich T (2014) Vulnerability assessment for reinforced concrete buildings exposed to landslides. *Bull Eng Geol Environ* 73(2):265–289
- MOHURD (2010) Code for design concrete structures (GB 50010–2010). Chinese Construction Industry Press, Beijing (in Chinese)
- MOHURD (2012) Load code for the design of building structures (GB 50009–2012). Chinese Construction Industry Press, Beijing (in Chinese)
- Murray YD (2007) Users’ manual for LS-DYNA concrete material model 159 (No. FHWA-HRT-05-062)
- Negulescu C, Foerster E (2010) Parametric studies and quantitative assessment of the vulnerability of a RC frame building exposed to differential settlements. *Nat Hazard Earth Syst* 10(9):1781–1792
- Orr TL (2017) Defining and selecting characteristic values of geotechnical parameters for designs to Eurocode 7. *Georisk* 11(1):103–115
- Parisi F, Sabella G (2017) Flow-type landslide fragility of reinforced concrete framed buildings. *Eng Struct* 131:28–43
- Peduto D, Ferlisi S, Nicodemo G, Reale D, Pisciotta G, Gullà G (2017) Empirical fragility and vulnerability curves for buildings exposed to slow-moving landslides at medium and large scales. *Landslides* 14(6):1993–2007
- Quan Luna B, Blahut J, Van Westen CJ, Sterlacchini S, van Asch TW, Akbas SO (2011) The application of numerical debris flow modelling for the generation of physical vulnerability curves. *Nat Hazards Earth Syst* 11(7):2047–2060
- Tiwari B, Marui H (1999) Landslide investigation and prevention practice in Nepal. □□□□ 20:37–55
- Totschnig R, Fuchs S (2013) Mountain torrents: quantifying vulnerability and assessing uncertainties. *Eng Geol* 155:31–44

- Uzielli M, Nadim F, Lacasse S, Kaynia AM (2008) A conceptual framework for quantitative estimation of physical vulnerability to landslides. *Eng Geol* 102(3):251–256
- Uzielli M, Catani F, Tofani V, Casagli N (2015) Risk analysis for the Ancona landslide—II: estimation of risk to buildings. *Landslides* 12(1):83–100
- Vamvatsikos D, Kouris L, Panagopoulos G, Kappos A, Nigro E, Rossetto T, Lloyd TO, Stathopoulos T (2010) Structural vulnerability assessment under natural hazards: a review. Proceedings of COST action C26 final international conference on Urban habitat construction under catastrophic events, Naples, 17–18 Sep 2010, pp 711–723
- Wu JS, Tian LQ, Kang ZC, Zhang YF, Liu J (1993) Debris flow and its comprehensive control. Science Press, Beijing (in Chinese)
- Xiao T, Li DQ, Cao ZJ, Tang XS (2017) Full probabilistic design of slopes in spatially variable soils using simplified reliability analysis method. *Georisk* 11(1):146–159
- Yin Y, Li B, Wang W, Zhan L, Xue Q, Gao Y, Zhang N, Chen H, Liu T, Li A (2016) Mechanism of the December 2015 catastrophic landslide at the Shenzhen landfill and controlling geotechnical risks of urbanization. *Engineering* 2(2):230–249
- Zeng C, Cui P, Su Z, Lei Y, Chen R (2015) Failure modes of reinforced concrete columns of buildings under debris flow impact. *Landslides* 12(3):561–571
- Zhang S, Zhang LM, Li XY, Xu Q (2018) Physical vulnerability models for assessing building damage by debris flows. *Eng Geol* 247:145–158

H. Y. Luo · L. M. Zhang 

Department of Civil and Environmental Engineering,
The Hong Kong University of Science and Technology,
Kowloon, Hong Kong, China
Email: cezhangl@ust.hk

H. Y. Luo
e-mail: hluae@connect.ust.hk

L. L. Zhang
Department of Civil Engineering,
Shanghai Jiaotong University,
Shanghai, China